MEASURING AND MODELING VERTICAL CROSSHEAD VIBRATION IN API-618 RECIPROCATING COMPRESSORS

Brian Howard
Signal Processing Engineer
GE Bently Nevada
Minden, NV, USA

Charles Hatch
Principal Engineer
GE Bently Nevada
Minden, NV, USA

Gregory Yonker
Development Engineer
Dresser-Rand
Painted Post, NY, USA

Kevin Philips
Reliability Engineer
BP West Coast Products
Blaine, WA, USA

Brian F. Howard, PE, is a Signal Processing Engineer at GE Oil & Gas in Minden, Nevada. In this role he focuses on diagnostic algorithm development and research. Prior to coming to work with the technology team Brian was the Global Technical Leader for Reciprocating Machinery Diagnostics where he supported the product development process and provided diagnostic support to customers to solve problems with rotating and reciprocating machinery. Mr. Howard received a B.S. in Mechanical Engineering from the University of Houston and an M.S. in Electrical Engineering from the University of Washington. He is a member of ASME and IEEE.

Charlie Hatch is a Principal Engineer with GE Oil & Gas, where he helps develop diagnostic solutions and new technology for Bently Nevada products. He has extensive experience in rotordynamics modeling and rotating machinery diagnostics. He has also developed diagnostic training materials and has instructed at many international training seminars. Charlie has authored a book on rotating machinery diagnostics and is the author of many technical papers. He holds B.S. and M.S. degrees in Mechanical Engineering from the University of California at Berkeley.

Gregory Yonker has a B.S. in Mechanical Engineering from Pennsylvania State University. He is a Research and Development Engineer at Dresser-Rand's Painted Post, New York operations. His work centers around the design and application of reciprocating compressors.

Kevin Phillips, PE is a Rotating Equipment Reliability Engineer at BP Cherry Point Refinery located in Blaine, Washington. His core responsibilities include monitoring, evaluation, maintenance, repair, selection, and upgrading rotating equipment to maximize equipment availability and performance. Kevin has been a Reliability Engineer at BP for 15 years. Prior to that he worked for a local engineering contractor for the oil industry for 5 years. Mr. Phillips received a B.S. in Mechanical Engineering from the University of Washington.

ABSTRACT

Reciprocating compressors constructed to API-618 standards find application in refineries, petrochemical plants, and pipelines around the world. These compressors are constructed with a force-fed lubricated crosshead that drives a double-acting piston via a piston rod. Looseness in the running gear (piston assembly, connecting rod assembly, and crosshead assembly) results in knocks (impulse events) that are usually detected at the crosshead guide with accelerometers and, in some cases, with proximity probes measuring the piston rod vibration at the pressure packing case. Crosshead guide accelerometers have proven successful in detecting and preventing catastrophic failure; however, the alarm set points for the vibration levels have been derived heuristically because no model exists that relates forces and impacts within the running gear to the vibration of the crosshead guide. This paper presents a model of the crosshead system that estimates the vibration response of the crosshead and crosshead guide in reaction to the forces and impulses in the running gear. The model incorporates the oil-film behavior including non-linear, position-dependent stiffness and damping. The paper also examines the system response in the time domain and the complex plane (eigenvalue migration). The numerical model results are validated by comparison with data acquired on operating machines in known conditions of distress. The results

show good agreement between the model and crosshead and piston rod vibration data, both in the timing and amplitude of vibration. Using the results of the model and historical data collected from operating reciprocating compressors the paper concludes with guidelines for filtering of crosshead accelerometer signals and alarm thresholds.

INTRODUCTION

Reciprocating compressors provide compression service in many applications throughout industry. This paper focuses on the large, slow speed units found in refining and petrochemical plants. These units are typically built to the American Petroleum Institute (API) Standard 618 and include some level of condition monitoring instrumentation. Crosshead guide acceleration and piston rod vibration are two commonly used measurements for condition monitoring (Schultheis and Howard (2000) and Schultheis et. Al. (2007)). Events in the cylinder can result in impulse events in the crosshead guide acceleration signal while events in the crosshead can change the piston rod vibration signal at the pressure packing case. In some cases, this cross coupling makes it difficult to determine the source of an impulse event or vibration signal.
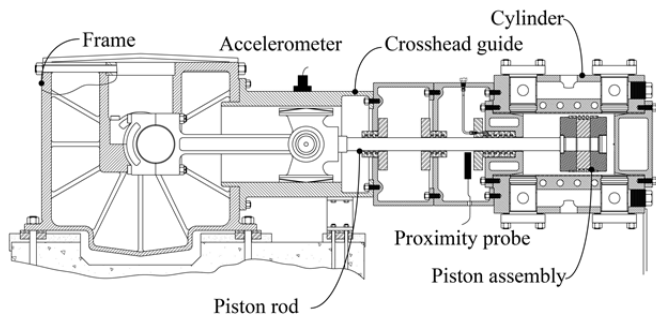

Figure 1. Sketch showing location of crosshead guide accelerometer and proximity probes ("rod drop" or "rod position" probes) at the pressure packing case.

Detection of malfunctions could be improved if the influence of the crosshead could be quantified. Prior work seems to have focused on pistons in internal combustion engines (Wilson and Fawcett, 1974). In this paper a model is developed for the crosshead motion as a function of rod load and crank-slider kinematics. This model is combined with a non-linear system of springs and dampers to simulate the response of the oil film and crosshead guide. The output of the model includes the system natural frequencies, crosshead displacement, and crosshead guide velocity. This latter output can be numerically differentiated and filtered to arrive at an estimated crosshead guide acceleration signal which can be compared to the measured crosshead guide acceleration signal to validate the model.

MODEL DEVELOPMENT

Figure 2 shows the nomenclature for the crank-slider mechanism in a typical API-618 process compressor. The crosshead lubrication results in an oil film between the crosshead shoes and the crosshead guide. The forces acting on the crosshead include gravity and the reaction force to the load
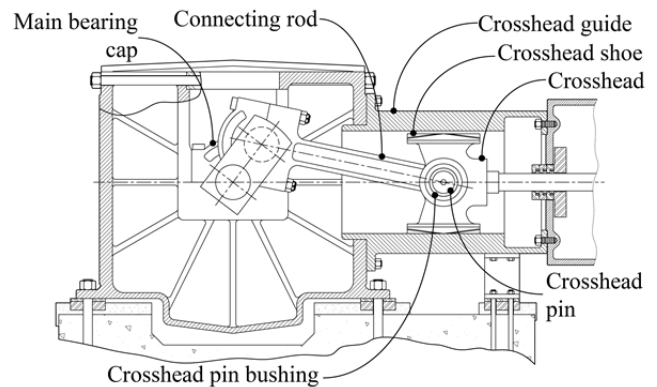

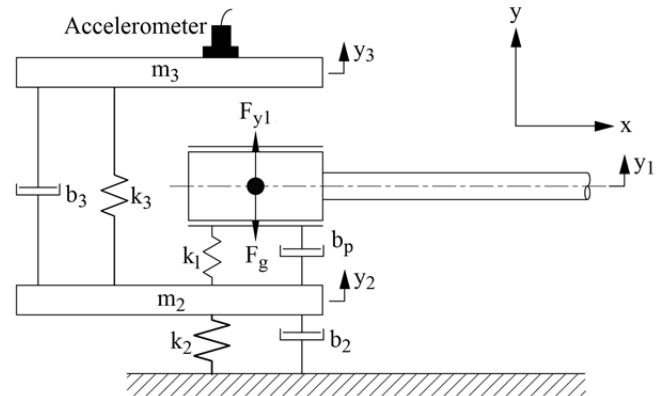Figure 2 - Reciprocating compressor crank-slider nomenclature.

Figure 3 - Schematic of crosshead support system for downrunning condition.
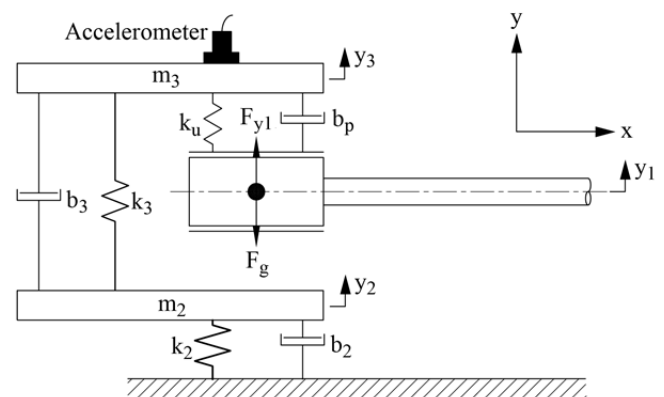

Figure 4 - Schematic of crosshead support system for uprunning condition.

on the connecting rod, which is also related to the measured cylinder pressures of the machine.

When the vertical force, F_{y1}, is less than the static weight, the crosshead accelerates towards the lower guide. Figure 3 shows the schematic for this condition. (It is assumed that the piston rod provides sufficient stiffness to neglect the rotation of the crosshead).

When the vertical force exceeds the static weight the crosshead accelerates towards the top guide. When the crosshead rises above the midpoint the model switches to the schematic shown in Figure 4. The simulation switches between the two models depending upon the location of the crosshead within the guides.

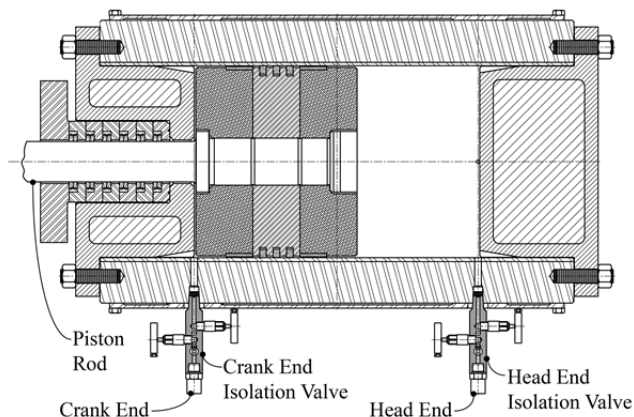The oil film has little influence on the crosshead motion

Figure 5 - Pressure transducer arrangement on typical API-618 cylinder.

until it nears either the upper or lower guide. In between neither the upper or lower oil film provides much support. In addition, the horizontal speed of the crosshead results in some variation in stiffness as the crosshead speed varies from maximum to minimum throughout the stroke. These characteristics mean that both the stiffness and damping values of the oil film depend on the horizontal speed of the crosshead as well as relative vertical displacement. Appendix A provides the details on the system model, including the equations of motion for the crosshead.

MODEL EVALUATION – COMPRESSOR FR66

Prior to model evaluation, data must be collected on the reciprocating compressor. Typically API-618 compressors have double-acting cylinders, meaning that compression occurs on both faces of the piston. Pressure transducers have to be installed on both ends of the cylinder, as shown in Figure 5. All transducers (pressure transducers, crosshead guide accelerometers, proximity transducers, etc.) are connected to an on-line protection and monitoring system, allowing for simultaneous data collection across all sensors. The monitoring system stores the waveforms if there is an alarm, if a defined amount of time has passed, or if the user requests it.

In addition to the measurements, the reciprocating masses, connecting rod weight, stroke, and other kinematic parameters must be recorded from the compressor manual, API data sheets, or measured in the field. Table C1 in Appendix C shows these values, along with the final non-linear stiffness and damping parameters.

With the data collection complete, the model evaluation can begin. The motivation for the model began with an observation of an impulse event in the filtered crosshead acceleration signal of a hydrogen make-up compressor (designated as FR66, throw #4). The frame rotates CCW and throw #4 is on the right side, as looking driver to driven. This throw is nominally an uprunning crosshead. Figure 6 shows a sample of the waveform data. The impulse event of interest is highlighted by a red rectangle and it appears in both the unfiltered (gray) and filtered (purple) crosshead acceleration signal.

The impact event had a high amplitude level, over 2g's pk in some cases, and did not align with combined rod load crossings, gas load crossings, or valve open/close events. The
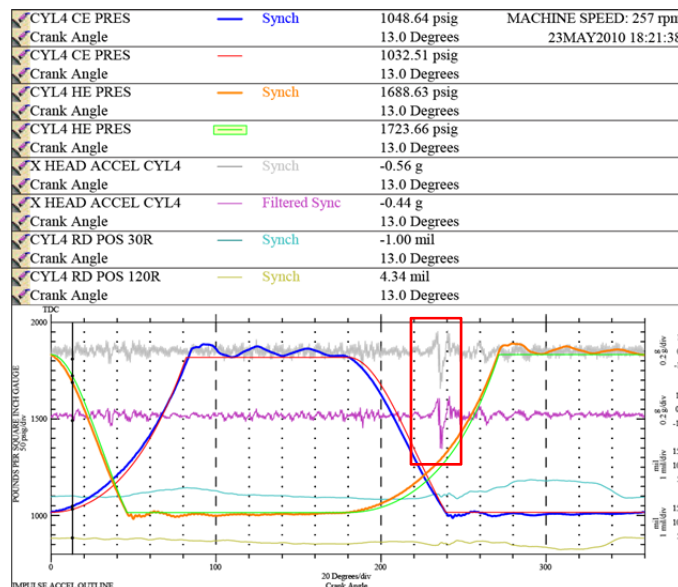

Figure 6 - Cylinder pressure, crosshead acceleration, and piston rod vibration.
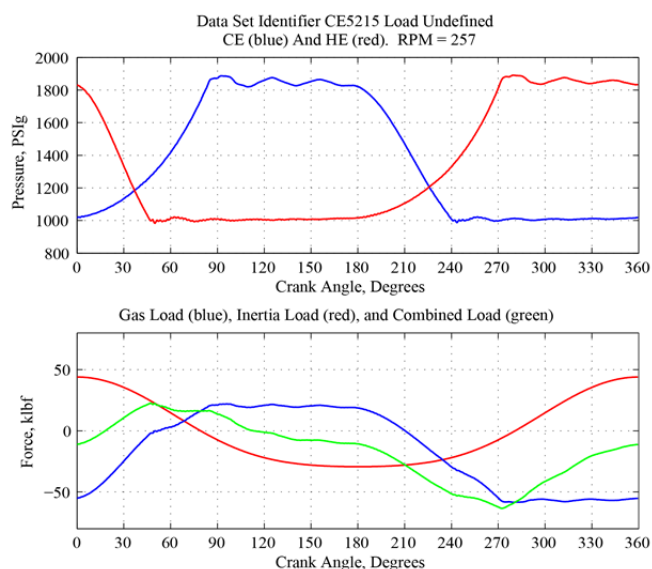

Figure 7 - Indicated pressure and rod load curves, full load and full pressure for compressor FR66, throw #4.

event did change crank angle position with load suggesting a cause in the running gear, possibly in the crosshead transition from one guide to another since the throw was uprunning.

Figure 7 shows the indicated pressure curves in the top pane and the rod load curves in the bottom pane. The indicated pressure curves were exported from the condition monitoring system. The inertia load curve (red line) was generated using Equation B9, the gas load curve (blue line) was calculated by multiplying the piston area times the pressure for both ends, and the combined load curve (green line) was calculated using Equation B10.

The combined rod load and running gear kinematics can be used to calculate the vertical force at the crosshead pin due to rod load using Equation B13. This is the black line in the top pane of Figure 8. The red line in the same pane represents the vertical force at the crosshead pin due to the connecting rod inertia and is calculated using Equation B29. The bottom pane
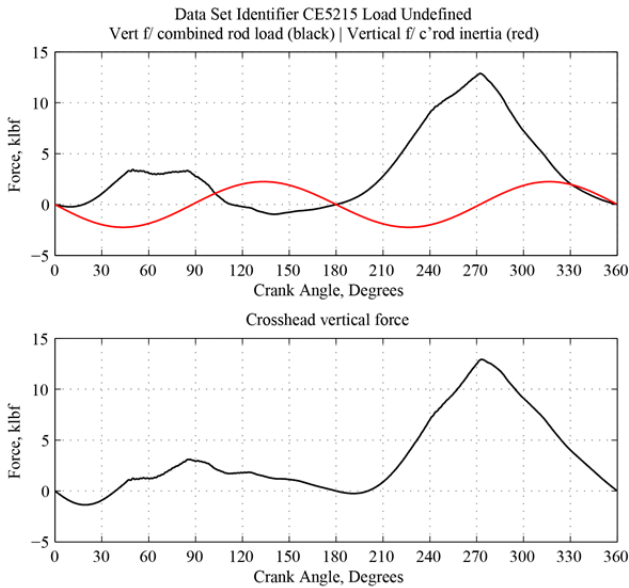
Figure 8 - Vertical forces at the crosshead pin for compressor FR66, throw #4.
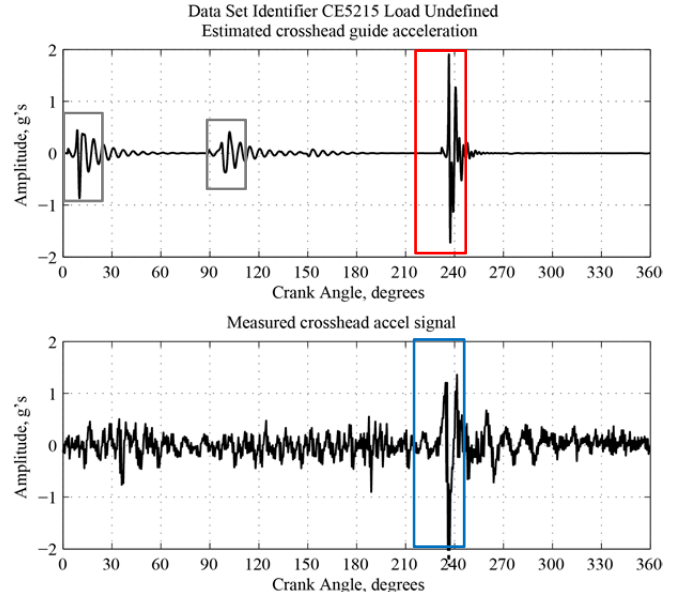

Figure 10 - Estimated crosshead guide vibration (top) and measured crosshead acceleration (bottom) for compressor FR66, throw #4.
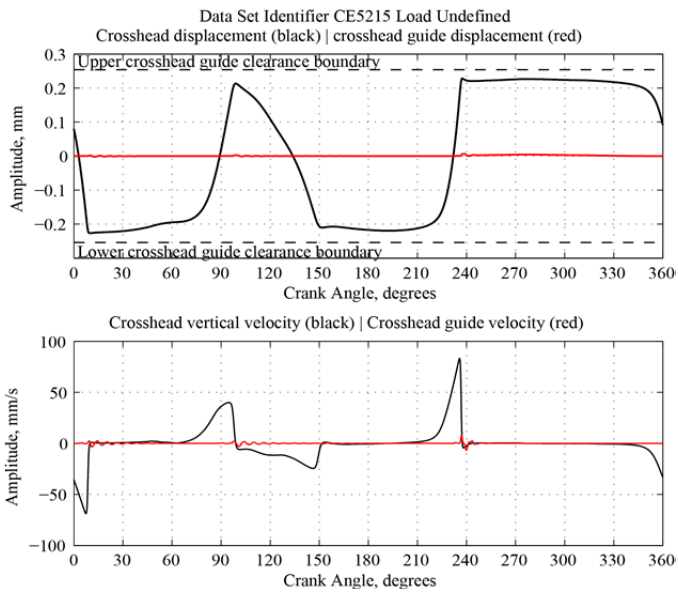

Figure 9 - Crosshead displacement, crosshead guide displacement, crosshead velocity, and crosshead guide velocity outputs from the model (compressor FR66, throw #4).
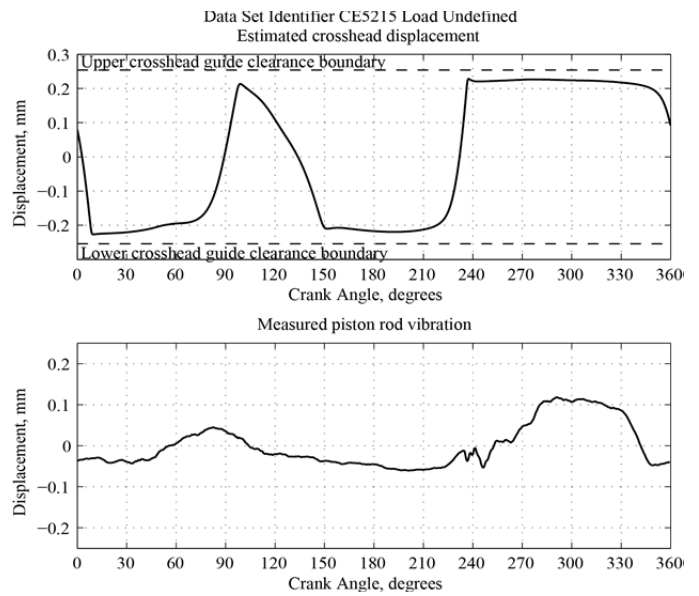

Figure 11 - Calculated crosshead motion (top) and measured piston rod vibration in the vertical plane (bottom), full load and full pressure (compressor FR66, throw #4).

shows the summation of these two forces calculated via Equation B30. This curve in the bottom pane is the input force to the model, F_{y1}.

Figure 9 shows selected outputs from the model. The top pane shows y_1, the crosshead vertical position, as the black line. The red line shows the upper crosshead guide position, y_3. The bottom pane shows y_1' and y_3', the crosshead and crosshead guide velocities.

The model output is compared to measurements made on the compressor. The crosshead guide accelerometer is closest to the crosshead and is less influenced by events in the cylinder so it can serve as the primary validation measurement. The estimated crosshead guide acceleration signal is calculated by numerically differentiating the crosshead guide velocity, then bandpass filtering the signal to match the characteristics of the

transducer and monitoring system. This estimated crosshead acceleration signal can be compared directly to the measured crosshead guide signal. The non-linear stiffness and damping parameters must be tuned so that the estimated crosshead guide acceleration matches the measured crosshead guide signal at varying loads. Figure C1 shows the stiffness and damping curves from this tuning.

With the model parameters determined, the model output (top pane of Figure 10) can be compared with the measured crosshead acceleration signal (bottom pane of Figure 10). The large impulse event, at about 240° after top dead center, can be seen in the measured crosshead guide acceleration signal and is highlighted by a blue box. The estimated crosshead guide acceleration signal shows a corresponding event at the same crank angle location, highlighted by a red box. The estimated signal also shows two other low amplitude events (~0.5 g's pk)
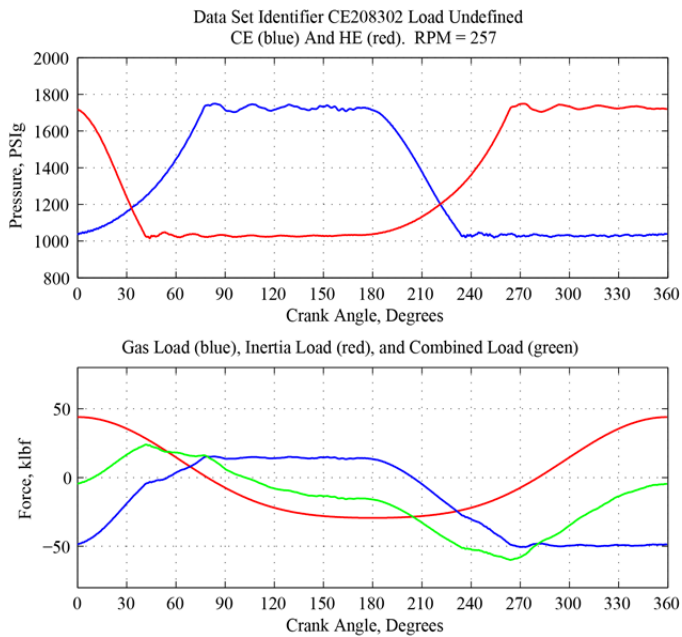
Figure 12 - Indicated pressure and rod load curves, reduced pressure (compressor FR66, throw #4).
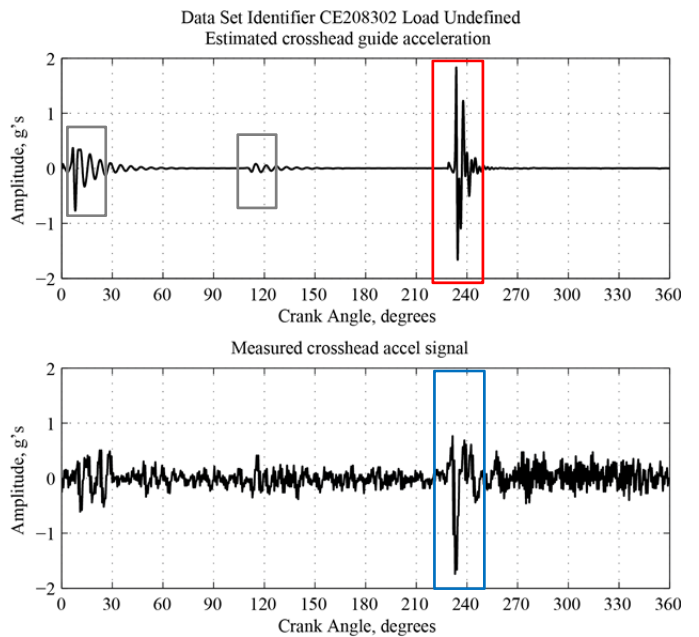

Figure 13 - Calculated crosshead guide vibration (top) and measured crosshead acceleration (bottom), full load and reduced pressure (compressor FR66, throw #4).

indicating minor impact events, not much higher than the noise floor of the measured accelerometer signal.

The model also provides an estimate of the crosshead position within the crosshead guide. The top pane of Figure 11 shows this position as a function of crank angle. At about 240° the model shows the crosshead energetically contacting the upper guide. This coincides with the timing of the impulse event in the measured crosshead acceleration signal.

In addition to checking the crosshead acceleration, the crosshead displacement can also be compared to the piston rod vibration signals collected by the proximity probes at the pressure packing case. Since these probes are farther away from the crosshead (and influenced by the piston motion inside the cylinder) the correlation between piston rod vibration and crosshead motion will not be as close as between the estimated and measured crosshead acceleration signal. The bottom pane of Figure 11 shows this measured piston rod vibration. It has large upward movement when the crosshead transitions from the lower to upper guide. This is good evidence that the model is accurately approximating the response of the crosshead system.

In the preceding section the compressor was fully loaded. Next, results will be examined at full load, but lower discharge pressures. Figure 12 shows the cylinder pressure and rod load curves. In this operating mode the cylinder discharge pressure is only 1700 PSIg [117 bar] compared to 1800 PSIg [124 bar] in the previous data set.

The pressure change is not large in terms of percentage; however, it has an effect on the model output and the measured crosshead acceleration. Figure 13 shows the estimated and measured crosshead acceleration signal for this load. The first small event in the estimated crosshead acceleration signal appears similar in both Figure 13 and Figure 10. The second event has nearly disappeared from the estimated crosshead acceleration signal. The third, and largest, event has shifted left by 3° in both the estimated and measured crosshead acceleration signals. This close tracking of events in both the
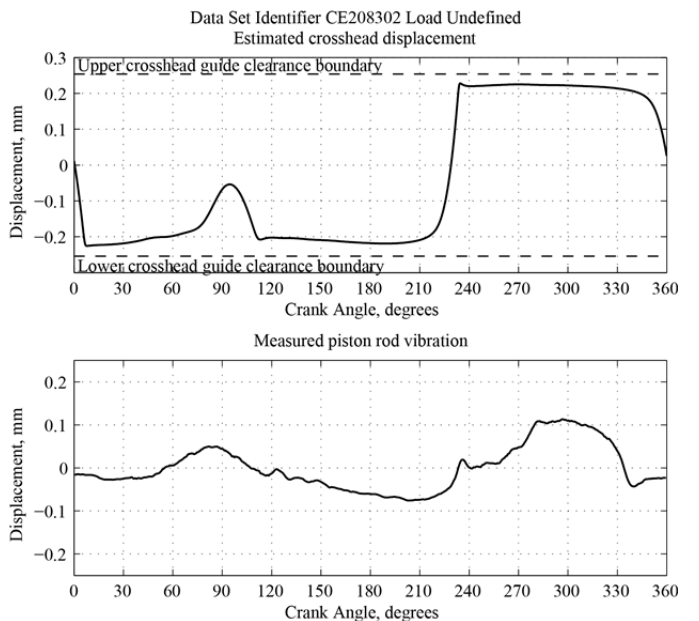
Figure 14 – Calculated crosshead motion (top) and measured piston rod vibration (bottom), full load and reduced pressure (compressor FR66, throw #4).

estimated and measured signal indicates the model approximates the physical system.

The calculated crosshead displacement, shown in the upper pane of Figure 14, still indicates energetic contact between the crosshead and upper guide, but also shifted left by 3°. This correlation provides more evidence that the impulse event in the measured crosshead acceleration signal is related to the crosshead contacting the upper guide. The estimated crosshead position and the piston rod vibration, shown in the lower pane of Figure 14, appear similar. From 60° to 120° both signals show an upward movement. From 210° to 240° both signals
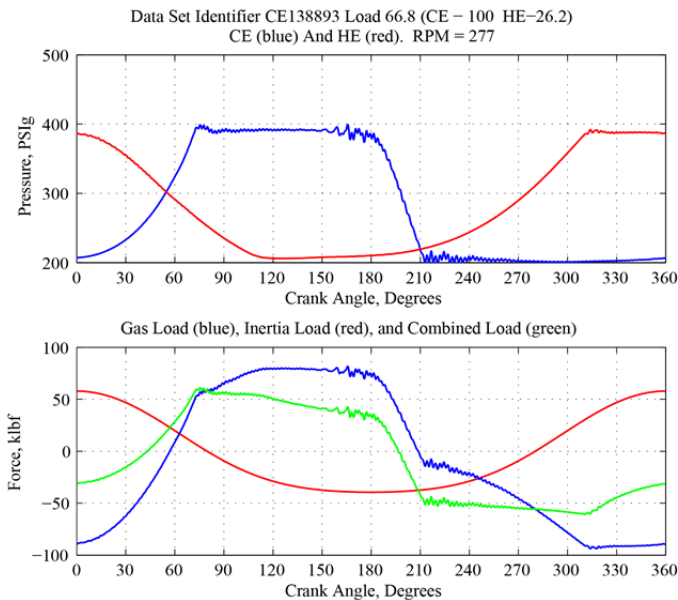
Figure 15 – Indicated pressure and rod load curves at 66.8% load (compressor FR315, throw #2).

show a similar pattern of movement as well, although the piston rod vibration signal is lower in amplitude.

Similar results were obtained at other load steps on this compressor. Based on the results of the model, the customer decided to continue to operate the compressor. Over the next few years, the vibration gradually increased rising to nearly 3 g's pk. During a scheduled outage the crosshead to crosshead guide clearance was checked and found to be at the outer limits. The crosshead was re-shimmed back to recommended clearances and the compressor placed back in service. The clearance adjustment reduced the amplitude of the impulse event back to the levels shown in Figure 6 confirming that the impulse event results from the crosshead impacting the upper crosshead guide.

MODEL EVALUATION – COMPRESSOR FR315

The next compressor frame (FR315, throw #2) has a history of piston hop that makes the analysis more interesting. In contrast to FR66, this compressor has a higher rod load rating and runs slightly faster (277 RPM versus 257 RPM). Throw #2 is downrunning. The design includes suction bottle supports connected at the upper crosshead guide, resulting in a much larger upper guide mass (m_3) value than on the previous machine. Appendix C has the specifics of the frame as well as the non-linear stiffness and damping curves.

This compressor has eleven different load steps. The 66.8% load step had many alarm events so this step was selected to be modelled. Figure 15 shows the indicated pressure and rod load curves for the machine loaded at 66.8%. Both ends are loaded; however some pockets in the head end have been opened.

Figure 16 shows the estimated crosshead guide acceleration signal and the measured crosshead guide acceleration signal. The estimated signal shows three events, but only one is far enough above the noise floor to be of interest (highlighted by a red box). There is a corresponding event in the measured crosshead acceleration signal (highlighted by a
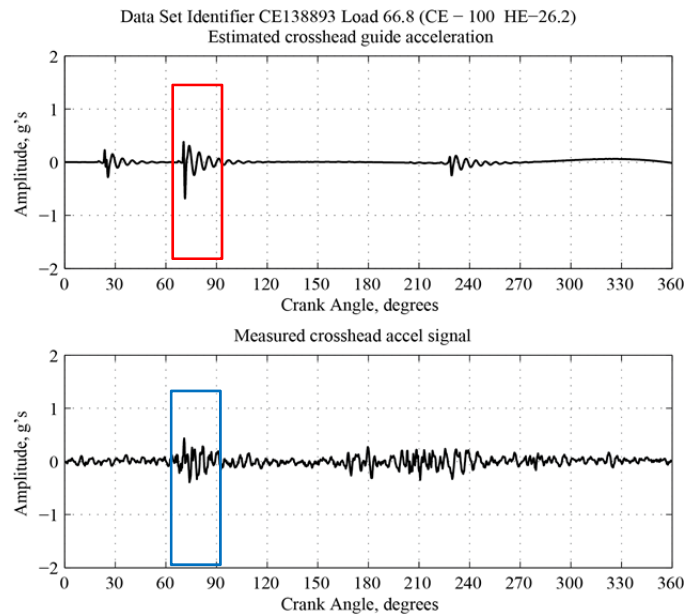

Figure 16 - Estimated crosshead guide vibration (top) and measured crosshead acceleration (bottom), 66.8% load (compressor FR315, throw #2.
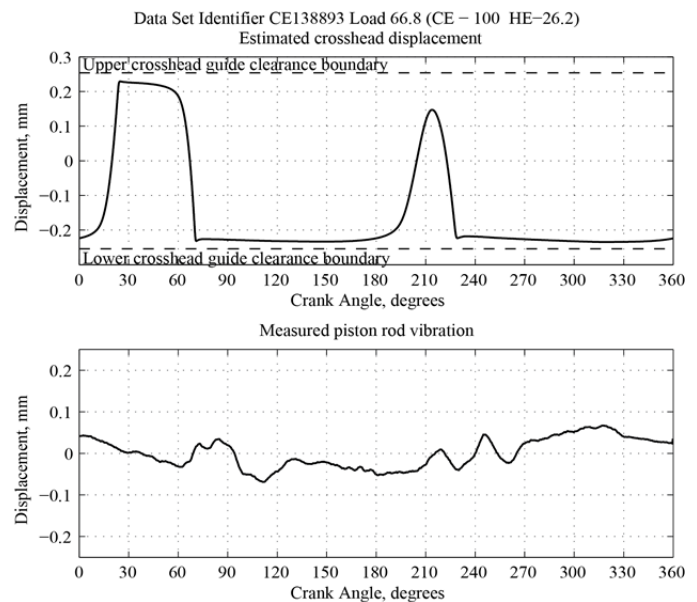

Figure 17 - Calculated crosshead motion (top) and measured piston rod vibration (bottom), 66.8% load (compressor FR315, throw #2).

blue box). The levels are low, but there seems to be reasonable correlation between the estimated and measured signal.

Comparing the calculated crosshead motion to the measured piston rod vibration signal, Figure 17, does not show good overall agreement. Given the reasonable agreement in the crosshead accelerometer signals this is unexpected. In fact, as the crosshead transitions down at about 65° the piston rod actually shows a small rise.

Although the piston motion does not correlate well with the estimated crosshead position, the measured vibration amplitudes are all at reasonable levels; however, seven seconds later the measured responses of both the crosshead accelerometer and piston rod vibration probes have increased significantly. The indicated pressures and rod loads, shown in
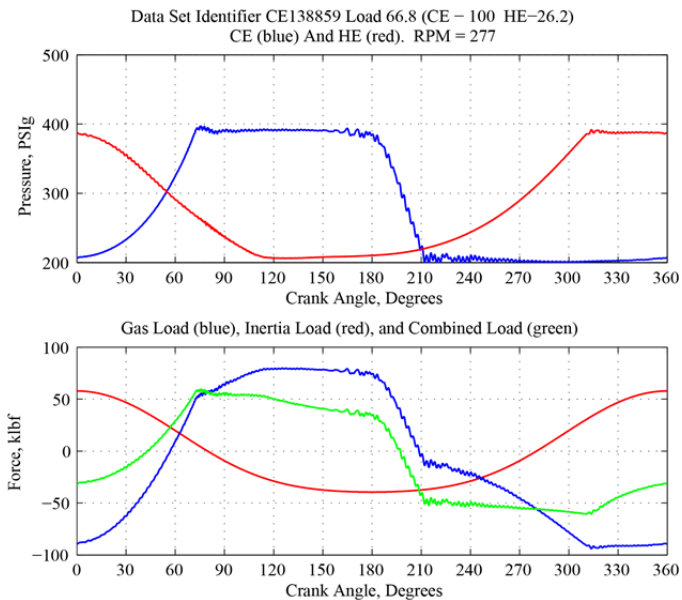
Figure 18 - Indicated pressure and rod load curves at 66.8% load (compressor FR315, throw #2). Data taken seven seconds after that shown in Figure 14.
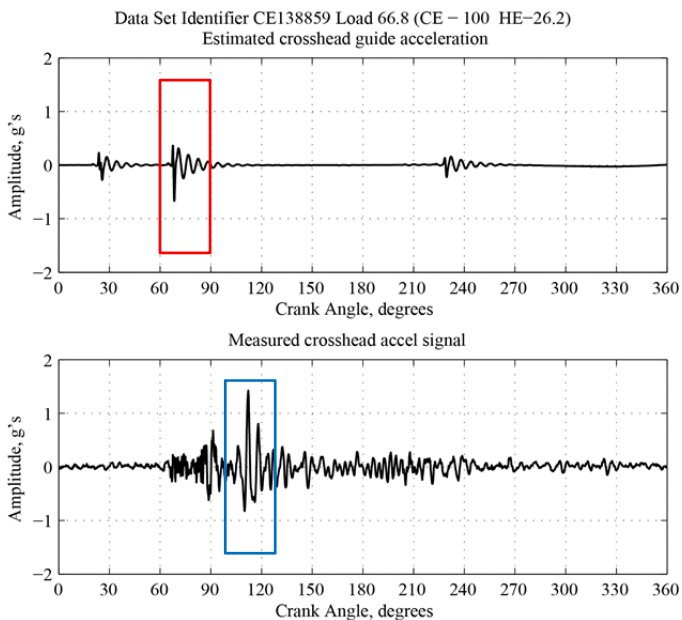

Figure 19 - Calculated crosshead guide vibration (top) and measured crosshead acceleration (bottom), 66.8% load (compressor FR315, throw #2).

Figure 18, appear virtually identical to that in Figure 15. That makes a change in load unlikely to be the cause of the vibration change.

Figure 19 shows the estimated crosshead guide acceleration and measured crosshead guide acceleration. The estimated crosshead guide acceleration appears identical to the previous case (top pane of Figure 16); however the measured crosshead guide acceleration differs greatly. In this case, there is a high amplitude event at 115°, highlighted by the blue box.

This event does not appear to relate to the events in the estimated crosshead guide acceleration, but does occur at the same time the piston rod vibration signal in Figure 20 shows high frequency vibration (also highlighted by a blue box).
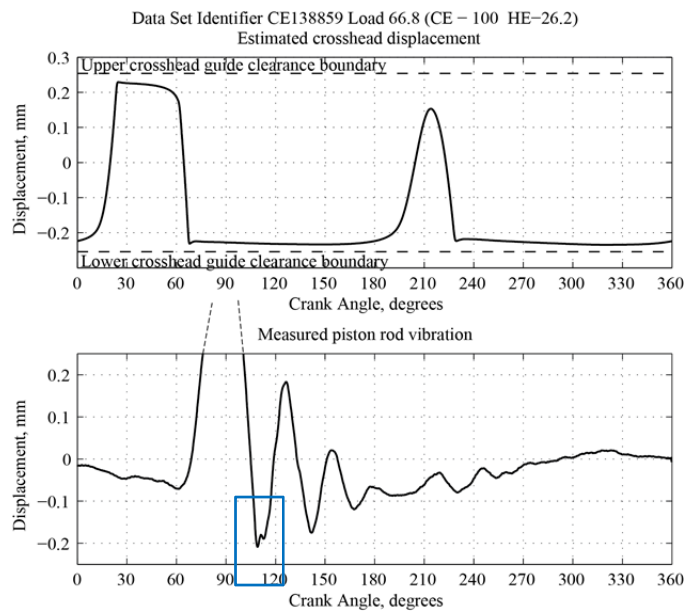

Figure 20 - Calculated crosshead motion (top) and measured piston rod vibration (bottom), 66.8% load (compressor FR315, throw #2).

Additionally, the calculated crosshead position (top pane of Figure 20) shows little resemblance to the measured piston rod vibration (bottom pane of Figure 20). In fact, the piston rod vibration shows a high amplitude event beginning at about 65° and peaking at about 90°. The large impulse event in the measured crosshead acceleration signal at 115° coincides with a sharp valley in the measured piston rod vibration signal, likely when the crosshead contacted the lower crosshead guide.

The large piston rod vibration is caused by piston hop. Liquids accumulate in the cylinder and, as the piston velocity increases, the liquid forms a wedge that lifts the piston assembly from the bottom of the cylinder. The lift and drag forces are largest when the piston velocity is highest. For this compressor the peak piston velocity can be found by substituting the machine parameters into Equation B8, setting it equal to zero, and solving for the crank angles. This results in velocity peaks at 79° and 281° after TDC. These are the points where the inertia curve (red line in the lower pane of Figure 18) crosses zero. If the force created by piston hop is large enough and rises fast enough, it can act as an impulsive force change to the loading on the crosshead and alter the crosshead position and the measured crosshead guide vibration. To understand why piston hop can have such an influence on the crosshead motion, the analysis has to shift from the time domain to the complex plane (eigenvalue analysis).

Appendix D provides an overview of system analysis in the complex plane. The poles of the system are the roots of the characteristic equation. For non-linear models the roots move, or migrate, in the complex plane. It is desirable to stay in the left hand plant and away from the imaginary axis (those systems turn into oscillators) and to be close to the real axis to have a well-damped system response. Since the poles are complex conjugates only the positive roots are shown in Figure 21. The plot only has labels for those eigenvalues with a non-zero imaginary component. All other eigenvalues without labels fall on the real axis (overdamped).
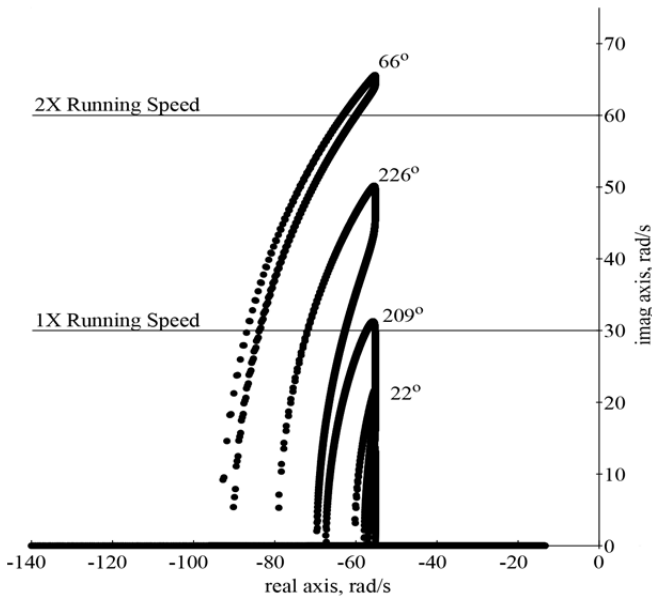
Figure 21 - Eigenvalue migration plot for the crosshead, 66.8% load (compressor FR315, throw #2).

Figure 22 – Crosshead damped natural frequency and piston velocity, 66.8% load (compressor FR315, throw #2).

The eigenvalues migration plot shows that the system has at least 4 crank angle bands in which the system has an underdamped response. In the complex plane it is hard to differentiate the different peaks. It would be helpful to correlate these results from the model with piston speed since piston hop is most likely to occur when the velocity of the piston is highest. To provide this correlation the damped natural frequencies (the projection of the eigenvalues on the imaginary axis) are plotted along with piston velocity in Figure 22.

The positive peak in the piston speed is very nearly at the some point in the revolution at which the system response has a large underdamped response. An impulse force to the crosshead at this point in the revolution would result in vibration of the
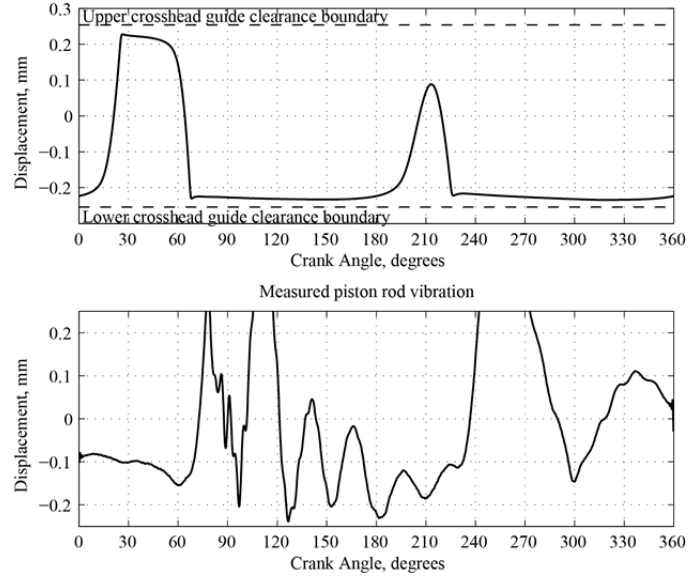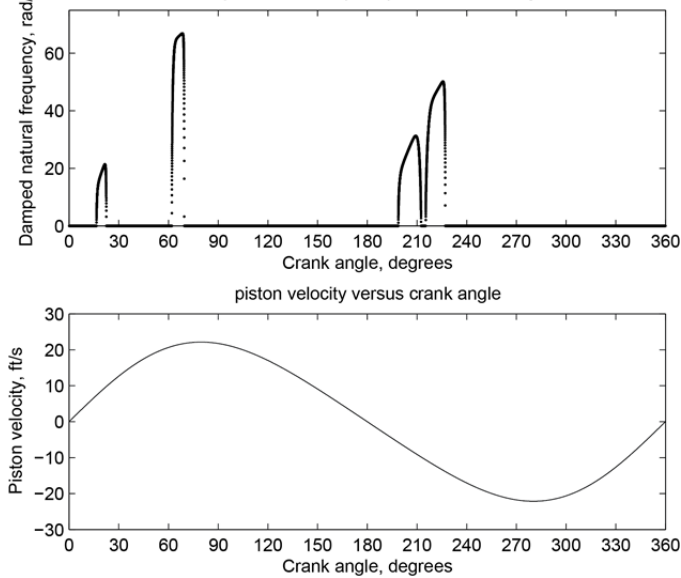

Figure 23 - Calculated crosshead motion (top) and measured piston rod vibration (bottom), 66.8% load (compressor FR315, throw #2).
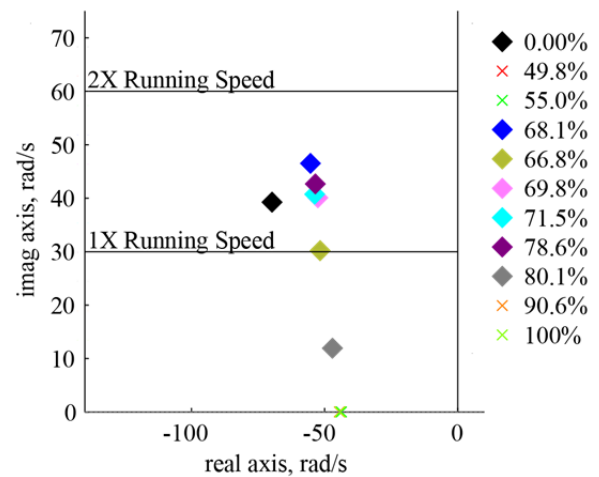
Figure 24 - Average eigenvalues in the 60° to 70° band as compressor load changes (compressor FR315, throw #2).

crosshead system. The correlation in timing between the peak damped natural frequency and the peak piston velocity suggests that as the lift and drag forces in the fluid wedge drive the piston upwards, it also imparts an impulsive force to the crosshead head system that results in vibration of the crosshead system and piston assembly.

The model also indicates a high damped natural frequency near 225°. This point is not as close to the maximum piston velocity; however, in some cases the condition monitoring system has collected data with a second piston hop beginning at this point. Figure 23 shows an example of this data. This data was acquired at the same load step as that Figure 20, but six months later. There is the first piston hop event starting at 60° and a second one starting at 225°. This provides more correlating evidence suggesting the vibration induced by piston hop is influenced by the crosshead system response.

Although the data has focused on the 66.8% load step, the

machine operates with multiple load steps. To simplify the presentation, average eigenvalues will be calculated between 60° and 70° for each load step. Figure 24 shows the imaginary part of these average eigenvalues. The model shows that load steps in this range of 66.8% to 80.1% do have eigenvalues with damped natural frequencies close to, or just above, the running speed of the compressor. These are the load steps where it would be expected to see piston hop. Although the model predicts piston hop at 0%, in this load step no gas is flowing through the compressor so no liquids can enter from process. Cylinder lubrication could accumulate, but the plant rarely operates the compressor unloaded for more than a few hours at a time.

Review of the historical condition monitoring data spanning twelve months of operation (~8,400 operating hours) found many instances of piston hop on this throw. Table 1 summarizes the results. The first column shows the load step, the second column shows the number of waveform samples that indicated a piston hop event had occurred, and the third column shows the number of operating hours at this load step. Since the compressor spends different hours at each load step, the last column shows a normalized value of events per thousand hours. Except for the 55% load step, the normalized event count generally increases the closer the average eigenvalue in Figure 24 is to the 1X running speed.

Table 1- Summary of piston hop events on FR315, throw #2

Load Step	Samples with piston hop event	Operating hours at this load	Normalized event count (events per thousand hours)
0.00%	0	8	0
49.8%	9	497	18
55.0%	173	950	182
68.1%	2	187	11
66.8%	114	284	402
69.8%	30	108	277
71.5%	45	167	270
78.6%	27	1496	18
80.1%	35	1278	27
90.6%	16	1820	9
100%	50	1579	32

It is worth taking a look at the data associated with the 55% load step. All but five of these events occurred in a single six-hour span of time. Figure 25 shows a sample of the estimated crosshead motion and measured piston rod vibration at this load. The measured piston rod vibration does have high vibration amplitude; however, it does not have the same shape as the piston hop event captured in Figure 20. The motion is more erratic and does not have the fast rise time and oscillatory response seen in Figure 20.
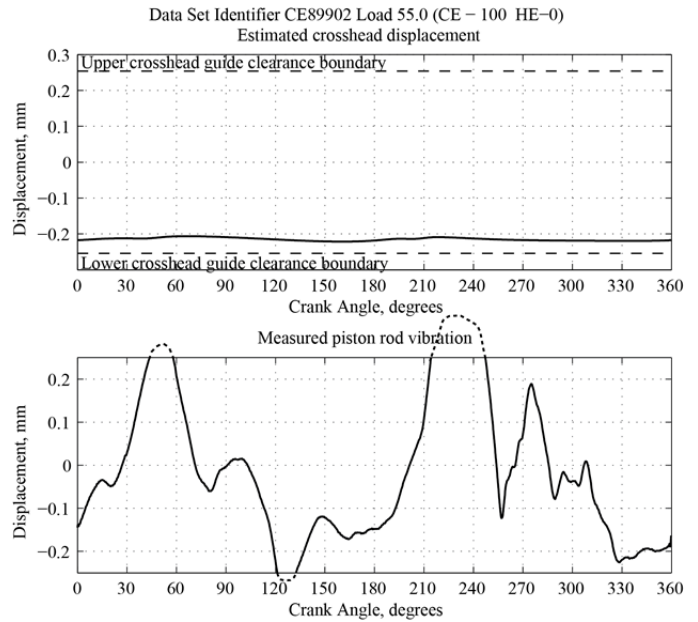

Figure 25- Calculated crosshead motion (top) and measured piston rod vibration (bottom), 55% load (compressor FR315, throw #2).

The difference in motion is likely due to the vertical loading on the crosshead at this step, shown in Figure 26. The throw is located on the right side of the machine and the crankshaft rotates CW, as viewed from the motor to the compressor. As the crank web rotates below the throw centerline, the connecting rod rotates about its center of mass and exerts an upward force on the crosshead pin. At the same time, pressure builds in the crank end chamber placing the piston rod in tension and exerting a downward force on the crosshead pin. As shown in the top pane of Figure 26, these two forces nearly cancel each other out resulting in a very lightly loaded crosshead. This is why the crosshead vertical force in the bottom pane of Figure 26 is almost zero. With such a lightly loaded crosshead the system has low stiffness and any forces acting on the piston assembly excite a larger response in the piston rod and crosshead. Looking at the bottom pane of Figure 25 it can be seen that the larger peaks occur as piston velocity reaches high values. This could be explained by liquid in the cylinder. Since the crosshead loading is low and the system stiffness is low the interaction of the piston and liquid results in high piston rod vibration, but not because a resonant response is excited as may be the case with the other load steps.
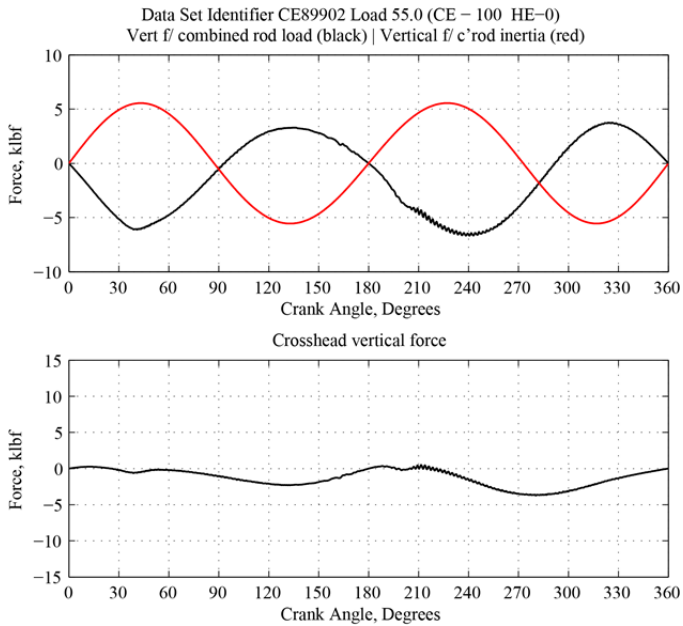
Figure 26 - Vertical forces at the crosshead pin (compressor FR315, throw #2).

APPLICATION TO PROTECTION SYSTEM INSTALLATION AND CONFIGURATION

With accurate results in the time and complex domains, the model seems to do a reasonable job of approximating the behavior of the crosshead and crosshead guide in response to loads and impacts. One of the advantages of a model, over a physical system, is that transducers can be placed anywhere on the model. This can be helpful in understanding how to locate the crosshead guide accelerometer.

Some OEMs and condition monitoring suppliers recommend that the crosshead guide accelerometer be mounted to the upper guide for uprunning crossheads and to the lower guide for downrunning crossheads where possible. One of the interesting results of the model is that very few reciprocating compressor throws operate as either uprunning or downrunning over all of the load steps and operating modes. That makes selection of the proper guide more difficult.

Since the model allows the transducers to be placed anywhere it is possible to plot the results with transducers located on the upper guide and lower guide. Figure 27 shows the estimated upper and lower crosshead guide acceleration signals for FR66, throw #4. Even though this was the throw with a large impulse event due to the crosshead contacting the upper guide, the model shows the lower guide had a higher amplitude response than did the upper guide. The difference comes about because the model has more damping between the guides than between the lower guide and the foundation so the lower guide has a higher damped natural frequency. The difference is not always so dramatic. In most of the cases the upper and lower crosshead guide acceleration signals have similar amplitudes. Thess model results suggest that placement of the accelerometer on either the upper or lower guide will provide good results, regardless of whether the crosshead is nominally uprunning or downrunning. This finding needs to be validated by checking the operating deflection shape (ODS) of crosshead guides on running machines.
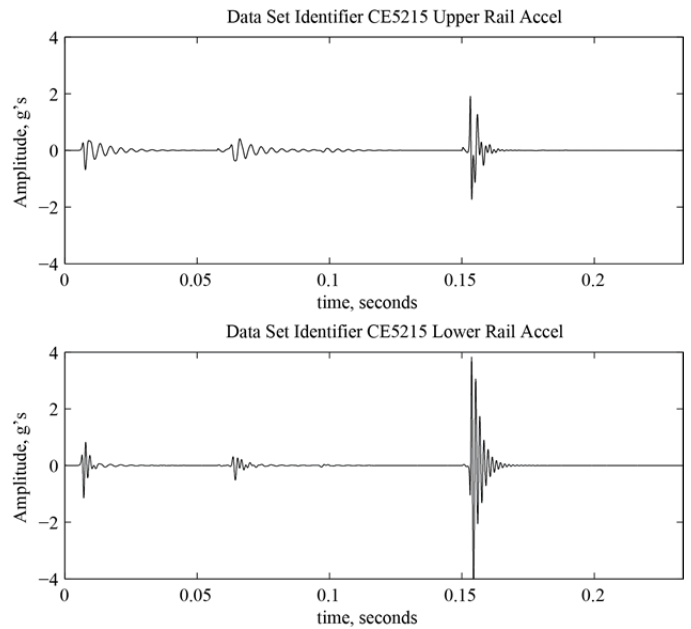

Figure 27 – Compressor FR66, throw #4 estimated upper crosshead guide acceleration (top pane) and estimated lower crosshead guide acceleration (bottom pane).

The model can also be used to validate configurations for machinery protection. Experience with the crosshead guide acceleration signal has shown that bandpass filtering the signal with a highpass corner of 3 hertz and a lowpass corner of 2000 hertz gives a signal that contains mechanical knock and impact information, but excludes the valve and flow noise information.

Figure 28 shows the spectral content from the unfiltered model output of Figure 13. The spectrum has most of the significant frequency content below 1000 hertz, although some does extend up to 1500 hertz. The spectra were similar for the other estimated crosshead guide acceleration signals suggesting that the empirically derived filter settings are reasonable starting points for detection of mechanical knocks and impacts.

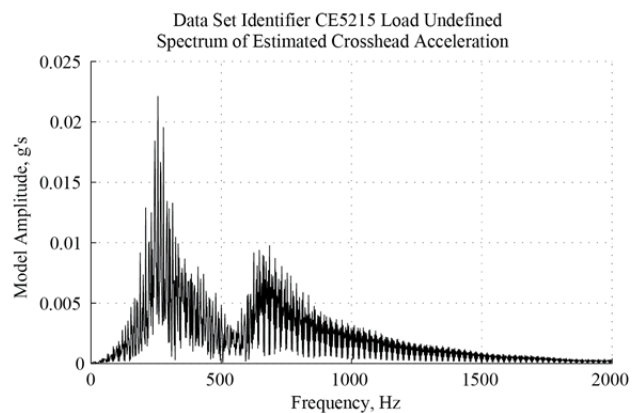Figure 28 - Spectrum of estimated crosshead guide acceleration (compressor FR66, throw #4).

The model also proves useful in assessing the amplitude of crosshead acceleration. From the preceding discussion it can be seen that estimated crosshead guide acceleration values below 0.5 g's pk typically do not show up in the measured crosshead guide acceleration signal. This suggests that the noise floor for

most API-618 machines is about 0.5 g's pk. This can be tested using historical data.

One of the authors (Howard) maintains a fault database that stores waveforms from a variety of condition monitoring platforms, both portable and on-line. Each waveform is reviewed and assigned a malfunction label. The database also includes waveforms from machines known to be in good condition. Figure 29 shows a histogram of the peak value for these waveforms. As was expected from the model, the center of mass of the histogram is near 0.5 g's pk. The historical data implies that for the typical healthy machine 0.5 g's is a reasonable noise floor for crosshead accelerometer event detection on API-618 machines.
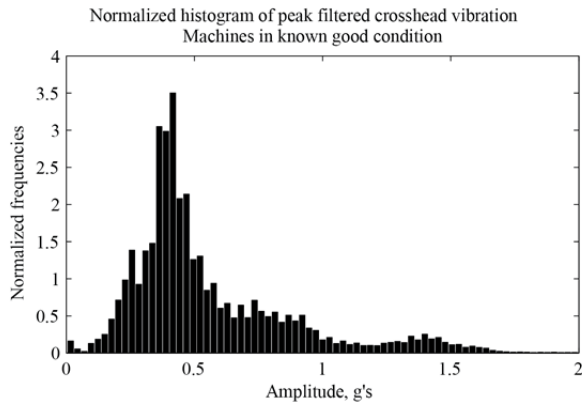

Figure 29 - Histogram of filtered crosshead acceleration peak values on API-618 machines in confirmed good condition.

When the estimated crosshead acceleration amplitude levels exceed 1.0 to 1.5 g's, the events amplitudes of the same level can almost always be seen in the measured crosshead acceleration signal. This suggests that amplitudes above this level for the filtered crosshead acceleration signal are related to mechanical impacts in the running gear. The impact may be an indication of machine distress (loose piston) or an operating characteristic of the machine (crosshead motion), but the root cause needs to be identified when the level is this high. This suggests that the alert thresholds in the range of about 1.5 g's pk are reasonable starting points for machines that have no OEM provided thresholds and that have no operating history.

These are a few examples of how the model and historical data can be used to validate settings on protection and condition monitoring systems.

CONCLUSIONS

This paper shows how a model was developed for the crosshead and crosshead guide system of API-618 reciprocating compressors. So long as forces acting at the piston come from the gas and inertia loads the model does a reasonable job of estimating the vibration response at the crosshead guide. Impulse forces acting on the piston assembly, such as piston hop, can alter the crosshead guide vibration response. Table 2 summarizes these findings.

Table 2 - Summary of estimated response from the model and measured response from the crosshead guide accelerometer.

Data Set	Est. Vib. (g's pk)	Meas. Vib. (g's pk)	Est. Location (°)	Meas. Location (°)	Reference Figure
FR66, Full Load	1.81	2.00	237	236	10
FR66, Low Press.	1.75	1.25	234	233	13
FR315, No Hop	0.53	0.41	70	71	16
FR315, Piston Hop	0.53	1.12	71	110	19

Application of this model to operating cylinders indicates that it provides useful information about both the vibration response at the crosshead guide as well as insight into interaction between the events in the cylinder and crosshead assembly. Future development and application of such models should result in an improved understanding of physical parameters (crosshead to crosshead guide clearance, oil flow, oil pressure, etc.) that can be adjusted to reduce vibration response and stress on reciprocating compressors.

NOMENCLATURE

r	Stroke/2
l	Connecting rod length
m_{cp}	Connecting rod crank pin mass
m_{cr}	Connecting rod crosshead pin mass
m	Mass of crosshead assembly, rod
m_{rec}	Reciprocating mass
m_2	Lower guide mass
m_3	Upper guide mass
F_{y1}	Vertical force from connecting rod
F_g	Gravitational force
b_p	Instantaneous oil film damping
b_n	Nominal oil film damping
b_e	Damping exponent
b_o	Damping offset
b_2	Damping, lower guide to foundation
b_3	Damping, upper guide to lower guide
k_l, k_u	Instantaneous oil film stiffness
k_n	Nominal stiffness exponent
k_e	Stiffness exponent
k_o	Stiffness offset
k_2	Stiffness, lower guide to foundation
k_3	Stiffness, upper guide to lower guide
ω	Rotational speed, radians/second

APPENDIX A – SYSTEM MODEL

The resultant vertical force on the crosshead arises from the connecting rod load combined with the angle of the connecting rod. For example, when the connecting rod is exactly parallel to the piston rod the resulting vertical force must be zero. Likewise, when the connecting rod is not parallel to the piston rod, there must be a resulting force in the vertical direction. Appendix B has more details on how this vertical force, F_{y1}, is calculated.

For the downrunning condition, the following equations can be derived (LaGrange notation is used for the derivatives and, unless otherwise stated, the independent variable is time, i.e. $y' = \dot{y} = dy/dt$):

$$my_1'' + y_1' b_p + k_l y_1 = F_{y1} - mg$$

$$m_2 y_2'' + k_2 y_2 + b_2 y_2' - k_l(y_1 - y_2) - k_3(y_3 - y_2) - b_p(y_1' - y_2') - b_3(y_3' - y_2') = -m_2 g$$

$$m_3 y_3'' + k_3(y_3 - y_2) + b_3(y_3' - y_2') = -m_3 g$$

Similarly, for the uprunning condition the following equations of motion can be derived:

$$my_1'' - y_1' b_p - k_u y_1 = F_{y1} - mg$$

$$m_2 y_2'' k_3(y_3 - y_2) - b_3(y_3' - y_2') + k_2 y_2 + b_2 y_2' = -m_2 g$$

$$m_3 y_3'' + k_3(y_3 - y_2) + b_3(y_3' - y_2') + k_u(y_3 - y_1) + b_p(y_3' - y_1') = -m_3 g$$

Where stiffness and damping have the following non-linear functions (where t=0 when the piston is at TDC):

$$k_l = k_u = k_n \cosh\left[(k_e\, d_y) + k_0\right](0.5 + (\sin[2\pi\omega t])^2)$$

$$b_p = b_n \cosh\left[(b_e\, d_y) + b_0\right]$$

These equations of motion are order-reduced and placed in state-space form. Equation 1A shows the state-space form for the downrunning case and Equation 2A shows the state-space form for the uprunning case.

$$
\begin{bmatrix} y_1'[t] \\ y_2'[t] \\ y_3'[t] \\ y_1''[t] \\ y_2''[t] \\ y_3''[t] \end{bmatrix} =
\begin{bmatrix}
0 & 0 & 0 & 1 & 0 & 0 \\
0 & 0 & 0 & 0 & 1 & 0 \\
0 & 0 & 0 & 0 & 0 & 1 \\
-\dfrac{k_l}{m} & 0 & 0 & -\dfrac{b_p}{m} & 0 & 0 \\
\dfrac{k_l}{m_2} & q1 & \dfrac{k_3}{m_2} & \dfrac{b_p}{m_2} & q2 & \dfrac{b_3}{m_2} \\
0 & \dfrac{k_3}{m_3} & -\dfrac{k_3}{m_3} & 0 & \dfrac{b_3}{m_3} & -\dfrac{b_3}{m_3}
\end{bmatrix}
\begin{bmatrix} y_1[t] \\ y_2[t] \\ y_3[t] \\ y_1'[t] \\ y_2'[t] \\ y_3'[t] \end{bmatrix} +
\begin{bmatrix} 0 \\ 0 \\ 0 \\ \dfrac{F_{y1}[t]}{m} \\ 0 \\ 0 \end{bmatrix}
$$

Eq. 1A

$$
\begin{bmatrix} y_1'[t] \\ y_2'[t] \\ y_3'[t] \\ y_1''[t] \\ y_2''[t] \\ y_3''[t] \end{bmatrix} =
\begin{bmatrix}
0 & 0 & 0 & 1 & 0 & 0 \\
0 & 0 & 0 & 0 & 1 & 0 \\
0 & 0 & 0 & 0 & 0 & 1 \\
-\dfrac{k_u}{m} & 0 & 0 & -\dfrac{b_p}{m} & 0 & 0 \\
0 & q3 & \dfrac{k_3}{m_2} & 0 & q4 & \dfrac{b_3}{m_2} \\
\dfrac{k_u}{m_3} & \dfrac{k_3}{m_3} & q5 & \dfrac{b_p}{m_3} & \dfrac{b_3}{m_3} & q6
\end{bmatrix}
\begin{bmatrix} y_1[t] \\ y_2[t] \\ y_3[t] \\ y_1'[t] \\ y_2'[t] \\ y_3'[t] \end{bmatrix} +
\begin{bmatrix} 0 \\ 0 \\ 0 \\ \dfrac{F_{y1}[t]}{m} \\ 0 \\ 0 \end{bmatrix}
$$

Eq. 2A

Where:

$$q1 = -\frac{k_2}{m_2} - \frac{k_3}{m_2} - \frac{k_l}{m_2}$$

$$q2 = -\frac{b_2}{m_2} - \frac{b_3}{m_2} - \frac{b_p}{m_2}$$

$$q3 = -\frac{k_2}{m_2} - \frac{k_3}{m_2}$$

$$q4 = -\frac{b_2}{m_2} - \frac{b_3}{m_2}$$

$$q5 = -\frac{k_3}{m_3} - \frac{k_u}{m_3}$$

$$q6 = -\frac{b_3}{m_3} - \frac{b_p}{m_3}$$

These equations were integrated numerically within MATLAB using ODE45. The state-space matrix was also used to extract the eigenvalues.

APPENDIX B – VERTICAL FORCES IN RECIPROCATING COMPRESSORS

Vertical forces on the crosshead arise as a result of the kinematics of the running gear, the inertia forces, and the gas load forces. Figure B1 shows the nomenclature associated with the running gear.
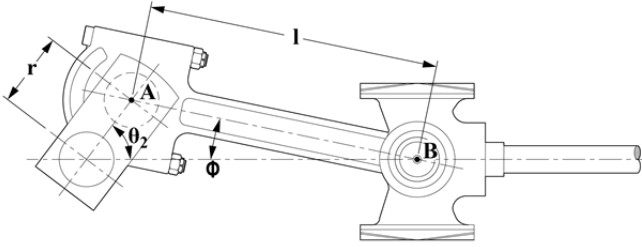

Figure B1 - Nomenclature used in kinematic analysis of reciprocating compressor crank slider assembly.

The kinematic analysis can be better understood if the crank-slider is reduced to a loop diagram in which vectors are substituted for the essential dimensions of the actual mechanical components. Figure B2 shows the nomenclature associated with the loop diagram and the relationship between the vectors and mechanical components.
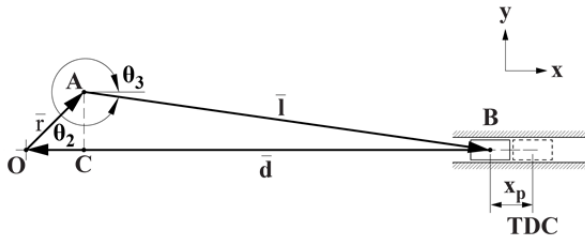

Figure B2 - Equivalent loop diagram of crank slider arrangement.

This system has the following nomenclature:
- r   Crank radius (1/2 of the stroke)
- $\theta = \theta_2$ Crank angle (0° at TDC), equals ω*t
- ω   Crankshaft speed in radians/second
- l   Connecting rod length
- $\phi = \theta_3$ Angle of the connecting rod
- d   Crankshaft centerline to crosshead centerline
- θ_4 Angle of vector $\bar{d}$, fixed at 180°
- x_p Distance from top dead center (TDC)

Begin the derivation by writing the loop equation from Figure B2 as:

$$de^{i\theta_4} + l\,e^{i\theta_3} + r\,e^{i\theta_2} = 0 \qquad \text{Eq. B1}$$

Since θ_4 is fixed at 180°, Equation B1 can be simplified and separated into real and imaginary parts:

$$-d + r\cos[\theta_2] + l\cos[\theta_3] = 0 \qquad \text{Eq. B2}$$

$$r\sin[\theta_2] + l\sin[\theta_3] = 0 \qquad \text{Eq. B3}$$

Equation B3 can be solved for the connecting rod angle, θ_3:

$$\theta_3 = -\text{asin}\left(\frac{r\sin[\theta_2]}{l}\right) \qquad \text{Eq. B4}$$

After some manipulation the distance from TDC to the current piston position can be written as:

$$x_p = r(1-\cos[\theta_2]) + l\left(1 - \sqrt{1 - \frac{r^2\sin[\theta_2]^2}{l^2}}\right) \qquad \text{Eq. B5}$$

To find the expression for velocity, return to Equation B1 and differentiate each element with respect to time:

$$e^{i\theta_4}d' + ie^{i\theta_2}r\theta_2' + ie^{i\theta_3}l\,\theta_3' + ie^{i\theta_4}d\,\theta_4' = 0 \qquad \text{Eq. B6}$$

Acceleration can be found by differentiating Equation B6 with respect to time:

$$\begin{aligned}
&-e^{i\theta_2}r\,(\theta_2')^2 - e^{i\theta_3}l(\theta_3')^2 + 2ie^{i\theta_4}d'\theta_4' - e^{i\theta_4}d(\theta_4')^2 \\
&+ e^{i\theta_4}d'' + ie^{i\theta_2}r\theta_2'' + ie^{i\theta_3}l\theta_3'' \\
&+ ie^{i\theta_4}d\theta_4'' = 0
\end{aligned} \qquad \text{Eq. B7}$$

After some simplification the acceleration can be expressed as:

$$d'' = -r(\theta_2')^2\left(\cos[\theta_2] + \frac{\frac{r^3}{l^3}\cos[\theta_2]^4 + \frac{r}{l}\left(1-\frac{r^2}{l^2}\right)\cos[2\theta_2]}{\left(1 - \frac{r^2\sin[\theta_2]^2}{l^2}\right)^{3/2}}\right)$$

$$\text{Eq.B8}$$

With the linear acceleration known, the scalar form of Newton's second law can be applied to find the reciprocating inertia load:

$$F_i = m_{rec}d'' \qquad \text{Eq. B9}$$

Combining the inertia load with the gas load results in a combined rod load expression of:

$$F_{rl} = F_i + F_{gas} \qquad \text{Eq. B10}$$

Since the connecting rod rotates at each end, the combined rod load results in a vertical force at the crosshead pin. Figure B3 shows how these forces interact. In this figure the crosshead pull to the right (tensile loading) and the connecting rod reacts upward and to the left. This connecting rod force, F_{cr}, can be resolved into a horizontal component (equal to and opposite of the combined rod load force, F_{rl}) and a vertical component.
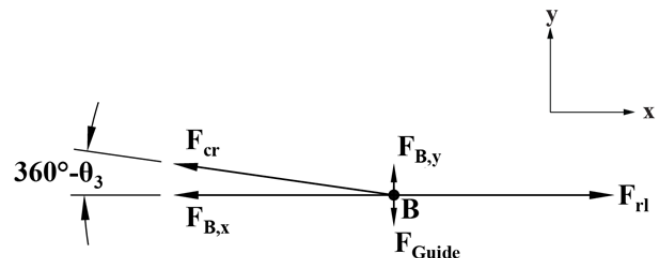

Figure B3 - Forces at the crosshead pin (point B in Figure B1 and B2).

From Figure B3 it can be observed that if the horizontal forces are summed and set to zero, the connecting rod force,

F_{cr}, can be expressed as a function of the connecting rod angle, $360° − θ_3$, and the combined rod load, F_{rl}:

$$\sum F_x = 0 \rightarrow F_{rl} + (−F_{cr}\cos[360° − θ_3]) = 0$$

$$F_{cr} = \frac{F_{rl}}{\cos[θ_3]} \qquad \text{Eq. B11}$$

The vertical force, $F_{B,y}$, can readily be expressed as:

$$F_{B,y} = F_{cr}\sin[360° − θ_3]$$

$$F_{B,y} = −\frac{F_{rl}}{\cos[θ_3]}\sin[θ_3]$$

$$F_{B,y} = −F_{rl}Tan[θ_3] \qquad \text{Eq. B12}$$

Since it is usually the crankshaft angle, $θ_2$, that is known, the vertical force is usually written by combining Equations B4 and B9 as:

$$F_{B,y} = −F_{rl}\tan\left[−asin[\frac{r\sin[θ_2]}{l}]\right]$$

$$F_{B,y} = F_{rl}\frac{r}{l}\frac{\sin[θ_2]}{\sqrt{1 − \frac{r^2}{l^2}\sin[θ_2]^2}} \qquad \text{Eq. B13}$$

The crosshead pin not only experiences vertical force due to the combined rod load, but it also experiences a vertical force as the connecting rod rotates about its center of mass. Most API-618 style connecting rods can be thought of as a slender rod joining a substantial bearing at each end. For this arrangement the center of gravity, G, can be approximately located as:

$$a = \frac{1}{3}l \qquad \text{Eq. B14}$$
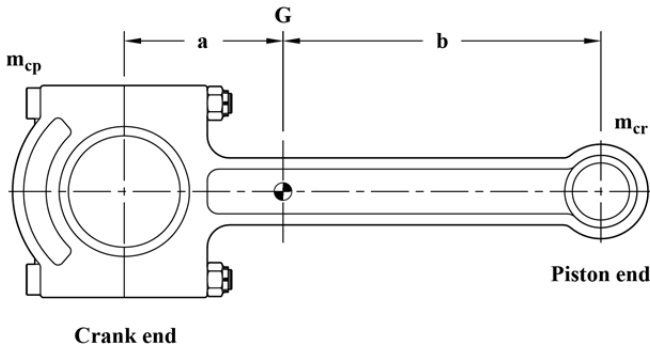
$$b = \frac{2}{3}l \qquad \text{Eq. B15}$$

Figure B4 - Connecting rod center of gravity.

The crank pin end mass, m_{cp}, and the crosshead pin end mass, m_{cr}, can be related to the center of gravity and the total connecting rod weight, m, by using Newton's second law.

$$m = m_{cp} + m_{cr} \qquad \text{Eq. B16}$$

$$\sum M_G = 0 \Rightarrow a\,m_{cp} − b\,m_{cr} = 0 \qquad \text{Eq. B17}$$

Use Equation B16 to eliminate the mass at the crosshead

end, m_{cr}, from Equation B17 and then solve for the mass at the crankpin end, m_{cp} :

$$m_{cp} = \frac{b}{a + b}m = \frac{b}{l}m \qquad \text{Eq. B18}$$

Equation B18 can be substituted directly into Equation B16 to find the mass at the crosshead end, m_{cr}:

$$m_{cr} = \frac{a}{a + b}m = \frac{a}{l}m \qquad \text{Eq. B19}$$

Derivation of the connecting rod reaction begins with a few assumptions to keep the analysis simple. These assumptions include:
1. No reciprocating mass (Equation B10 accounts for this)
2. Frictionless operation (only a vertical force is allowed at point B, the crosshead pin)
3. The crank turns counter-clockwise.

Figure B5 shows a sketch of the crank-slider, along with the associated nomenclature.
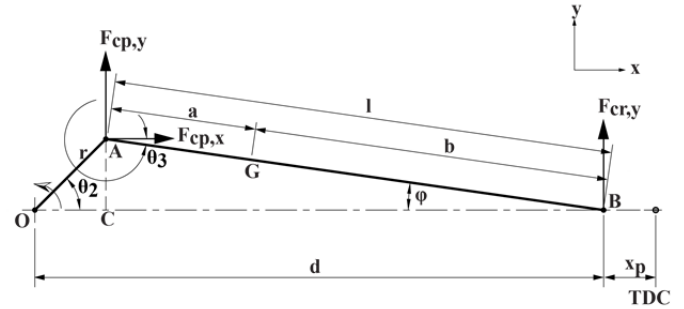

Figure B5 - Schematic of crank-slider with connecting rod inertia.

For this case of plane motion, the scalar form of Newton's second law can be used to sum the forces and the moments about the center of gravity, G, of the connecting rod.

$$F_{cp,x} = −m\,x_G'' \qquad \text{Eq. B20}$$

$$F_{cp,y} + F_{mcr,y} = −m\,y_G'' \qquad \text{Eq. B21}$$

$$−F_{cp,x}a\,Sin[θ_3] + F_{cp,y}a\,Cos[θ_3] − F_{cr,y}b\,Cos[θ_3] = I_G θ_3'' \qquad \text{Eq. B22}$$

In Equation B22, I_g indicates the rotational moment of inertia about the center of mass, G. The next step is to define the path of travel for the connecting rod center of mass. It travels in an elliptical path (Den Hartog, 1985) with the following expressions for displacement and acceleration:

$$x_G = x_p + (x_A − x_p)\left(\frac{b}{l}\right) = \frac{b}{l}x_A + \frac{a}{l}x_p \qquad \text{Eq. B23}$$

$$x_G'' = \frac{b}{l}x_A'' + \frac{a}{l}x_p'' \qquad \text{Eq. B24}$$

$$y_G = \frac{b}{l}y_A \qquad \text{Eq. B25}$$

$$y_G'' = \frac{b}{l}y_A'' \qquad \text{Eq. B26}$$

With three equations and three unknowns, each force can readily be found.

$$F_{cp,x} = m_{cp}x_A'' + m_{cr}x_B''$$ \hfill Eq. B27

$$F_{cp,y} = -\frac{a\,m_{cp}\,\tan[\theta_3]x_A''}{l} - \frac{a\,m_{cr}\,\tan[\theta_3]x_B''}{l} + \frac{b\,m_{cp}\,y_A''}{l} - \frac{i_G\theta_3''}{l\,\mathrm{Cos}[\theta_3]}$$ \hfill Eq. B28

$$F_{cr,y} = \frac{a\,m_{cp}\tan[\theta_3]x_A''}{l} + \frac{a\,m_{cr}\tan[\theta_3]x_B''}{l} + \frac{a\,m_{cp}y_A''}{l} + \frac{i_G\theta_3''}{l\,\mathrm{Cos}[\theta_3]}$$ \hfill Eq. B29

The total vertical force at the crosshead pin can be found by combining Equations B13 and B29:

$$F_{y1} = F_{B,y} + F_{cr,y}$$ \hfill Eq. B30

APPENDIX C – MODEL PARAMETERS

Table C1 – Model parameters for reciprocating compressor FR66, throw #4.

Parameter	Value	Units
r	254	mm
l	1276	mm
CE rod dia	102	mm
HE rod dia	0	mm
Bore dia	206	mm
Isent. exp.	1.37	-
m_{cp}	204	kg
m_{cr}	45	kg
m	868	kg
m_{rec}	887	kg
m_2	4000	kg
m_3	4000	kg
F_g	-9.8	N
b_n	1	N-s/m
b_e	70500	-
b_o	75000	-
b_2	5.5E+5	N-s/m
b_3	1.5E+6	N-s/m
k_n	1	N/m
k_e	8.6E+5	-
k_o	3.8E+6	-
k_2	4.8E+10	N/m
k_3	3.1E+10	N/m
ω	26.9	rad/s

Table C2 – Model parameters for reciprocating compressor FR315, throw #2.

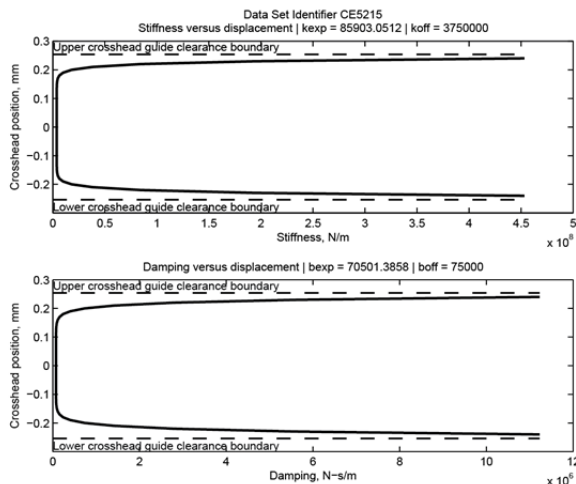| Parameter	Value	Units
r	229	mm
l	1219	mm
CE rod dia	127	mm
HE rod dia	0	mm
Bore dia	622	mm
Isent. exp.	1.46	-
m_{cp}	318	kg
m_{cr}	114	kg
m	680	kg
m_{rec}	1126	kg
m_2	8000	kg
m_3	24000	kg
F_g	-9.8	N
b_n	1	N-s/m
b_e	70500	-
b_o	75000	-
b_2	1.5E+6	N-s/m
b_3	2.4E+7	N-s/m
k_n	1	N/m
k_e	8.6E+5	-
k_o	3.8E+6	-
k_2	1.8E+11	N/m
k_3	1.5E+11	N/m
ω	29.0	rad/s

Figure C1 - FR66 throw #4 nonlinear stiffness and damping curves.
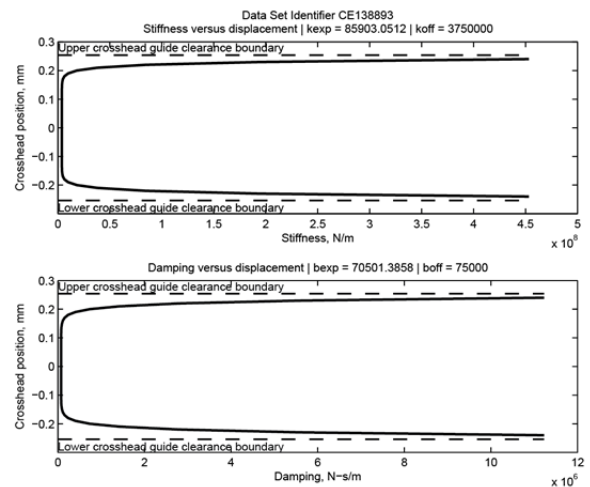

Figure C2 – FR315 throw #2 nonlinear stiffness and damping curves.

APPENDIX D – SYSTEM DYNAMICS IN THE COMPLEX PLANE

To show how the poles in the complex plane relate to mechanical behavior it is helpful to examine a second order system, such as the mass-spring-damper system of Figure D1. With no external forces, other than gravity, the mass is at rest. Now, someone comes along and pulls the mass downward, as indicated by the outline in Figure D1, and releases it. The spring will exert a force on the mass pulling it back to the equilibrium position. As the mass travels, its velocity increases. In fact, at the point of equilibrium the velocity will be at a maximum and momentum will carry the mass a distance of Δx above the equilibrium, where it stops, and begins to travel downward. It will again pass through the equilibrium point, but will not quite reach the starting point because of energy dissipated by the damper. The cycle with the mass travels a little less each cycle until it eventually comes to rest.
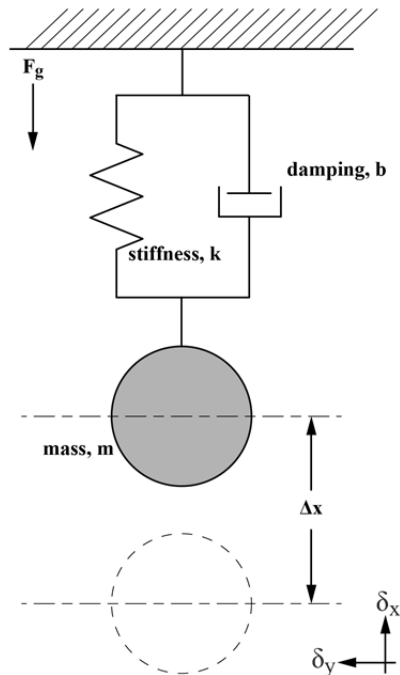

Figure D1 - Mass-spring-damper system

For this system, the forces in the vertical direction can be summed as:

$$\sum F_x = 0 \Rightarrow m\,\ddot{x}(t) = -k\,x(t) - b\dot{x}(t)$$

This can be written to normalize the coefficients by the mass:

$$\ddot{x}(t) + 2\,\zeta\,\omega_0\,\dot{x}(t) + \omega_0^2\,x(t) = 0 \qquad \text{Eq. D1}$$

$$\zeta = \frac{b}{2\sqrt{km}}, \qquad \omega_n = \sqrt{\frac{k}{m}}$$

One way to solve this equation is to use the Laplace transform. This transform allows Equation D1 to be written as a polynomial (capital letters are used to designate the variables in the Laplace transforms):

$$X(s) = \frac{\alpha\,s + \beta}{s^2 + 2\,\zeta\,\omega_0\,s + \omega_0^2} \qquad \text{Eq. D2}$$

The α and β terms are determined by the initial conditions of the system. The denominator of Equation D2 is called the *characteristic* equation. The roots of this equation describe the dynamic behavior of the system and can be written as:

$$s = -\zeta\omega_n \pm \sqrt{-\omega_n^2 + \zeta^2\omega_n^2} = -\zeta\omega_n \pm j\,\omega_n\sqrt{1 - \zeta^2}$$

These roots determine the transient and steady state response of the system. To understand how, it can be observed that the roots have real and imaginary parts. These parts can be plotted in the complex plane, as shown in Figure D2.
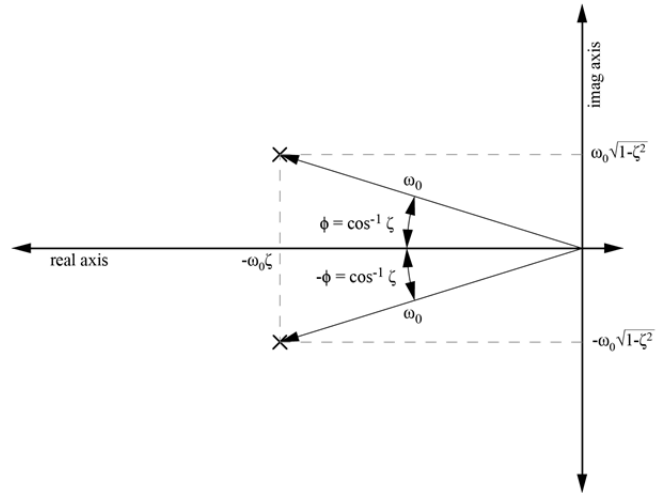

Figure D2 – Eigenvalues of the mass-spring-damper system plotted in the complex plane.

The roots, or eigenvalues, have a magnitude equal to the system's undamped natural frequency. Regardless of the damping ratio, if mass and stiffness remain constant, the system will always have the same undamped natural frequency. The damping ratio describes the angle between the undamped natural frequency and the real axis. The projection of the pole onto the imaginary axis gives the damped natural frequency.

For this simple model, the eigenvalues occur as complex conjugate pairs so displaying both pairs does not add much information to the plot. The convention when plotting the eigenvalues is to show only the positive value. Figure D3 shows the eigenvalue positions in the complex plane along with the system response. As the damping approaches zero, the poles move toward the imaginary axis. If the damping is zero, the poles will be on the imaginary axis and the system will behave as an oscillator. In contrast, as the damping ratio approaches unity, the poles move toward the real axis. If the damping ratio is unity, then the poles sit on the imaginary axis and the system is described as critically damped. This means that for free vibration the system converges to the equilibrium position as fast as possible without oscillation.
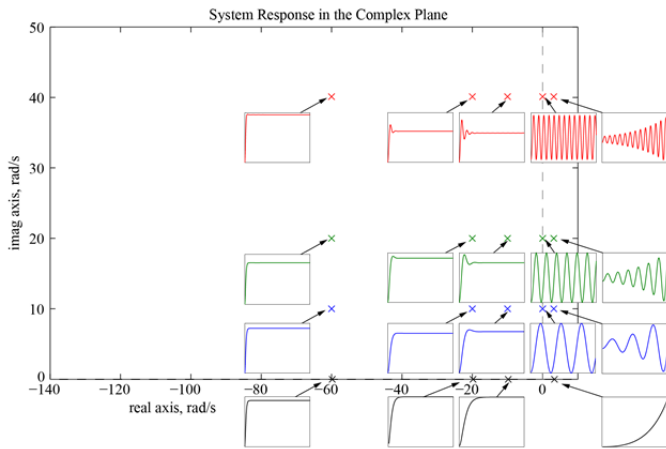
Figure D3 – System response in the complex plane.

The model of the crosshead system is more complex than the simple mass-spring-damper system used in this appendix; however, the basic ideas still apply. Because the model used for the crosshead system is non-linear, the methodology for calculating the eigenvalues is slightly different. At each step of the integration, the state-space matrices are saved. Once the simulation is compete, the eigenvalues are found for the state space matrices at each step of the integration. This is called a frozen-time approach and results in the eigenvalues as a function of crank angle. Plotting these eigenvalues results in the plot seen in Figure 21 of the main text of the paper. The imaginary parts (damped natural frequency) of these eigenvalues are plotted in Figure 22.

REFERENCES

API Standard 618, 2007, "Reciprocating Compressors for Petroleum, Chemical, and Gas Industry Services", Fifth Edition, American Petroleum Institute, Washington, D.C.

API Standard 670, 2014, "Machinery Protection Systems", Fifth Edition, American Petroleum Institute, Washington, D.C.

Schultheis, S. M., and Howard, B. F., "Rod Drop Monitoring, Does It Really Work?", Proceedings of the Twenty-ninth Turbomachinery Symposium, Texas A&M University, College Station, pp 11-20.

S. M. Schultheis, C. A. Lickteig, R. Parchewsky, "Reciprocating Compressor Condition Monitoring", Proceeding of the Thirty-sixth Turbomachinery Symposium, Texas A&M University, College Station, pp. 107-113, 2007.

R Wilson, J.N Fawcett, "Dynamics of the Slider-Crank Mechanism with Clearance in the Sliding Bearing", Mechanism and Machine Theory, Volume 9, Issue 1, Spring 1974, Pages 61-80.

Den, Hartog J. P. *Mechanical Vibrations,* New York: Dover Publications, 1985.